

CrossMark  
click for updatesCite this: *Phys. Chem. Chem. Phys.*,  
2016, **18**, 33068Received 16th August 2016,  
Accepted 10th November 2016

DOI: 10.1039/c6cp05681d

www.rsc.org/pccp

# A DFT study of the effect of SO<sub>4</sub> groups on the properties of TiO<sub>2</sub> nanoparticles†

Olga Miroshnichenko,<sup>\*ab</sup> Sergei Posysaev<sup>ab</sup> and Matti Alatalo<sup>a</sup>

We present a study of the optical, electronic, and structural properties of TiO<sub>2</sub> anatase-structured nanoparticles upon adsorption of SO<sub>4</sub> groups, which are always present on the surface of the particles during the sulfate manufacturing method. Structural and electronic properties were studied using the density functional theory method (DFT), and optical properties were obtained by time-dependent DFT. It was found that SO<sub>4</sub> groups alter both the geometric and electronic structure of TiO<sub>2</sub> nanoparticles and change the photoabsorption characteristics. In particular, we find that η<sup>2</sup>-O<sub>2</sub> type O–O moieties are formed due to the adsorption of 3 and 4SO<sub>4</sub> groups.

## 1 Introduction

TiO<sub>2</sub> is a popular semiconductor used in a huge number of applications, to name a few: photocatalysis and photocatalytic splitting of water,<sup>1–3</sup> pollutant removal,<sup>4,5</sup> pigments.<sup>6</sup> Such popularity comes from the stability, non-toxicity, and abundance of titanium dioxide. There are three natural polymorphs of titanium dioxide: rutile, anatase, and brookite, all having different lattice constants, slightly different structure and, therefore, properties. Rutile is the most popular TiO<sub>2</sub> polymorph due to its thermal stability.

With progress in nanotechnology, nanosized titanium dioxide finds application in many new areas, in addition to traditional ones, such as hydrogen generation,<sup>7,8</sup> biomedical implants,<sup>9,10</sup> solar cells,<sup>11–14</sup> and UV-protectors.<sup>8,15</sup> Nanoparticles possess the advantage of an increased surface-to-volume ratio, which is extremely plausible in the field of catalysis. The properties of small titanium dioxide particles are different from the bulk, and they are determined by their structure and size,<sup>16,17</sup> which depend on the environment and the manufacturing method.<sup>18</sup> Therefore, it is highly important to understand the properties of nanoclusters covered with adatoms and coatings. When the size of the nanoparticles is on the scale of several nanometers, anatase is the most stable structure.<sup>19</sup> Moreover, anatase is more stable than rutile at 0 K.<sup>20</sup>

In real life, nanoparticles always reside in some chemical environment. The effect of many different adatoms and coatings on the properties of TiO<sub>2</sub> nanoparticles has already been studied

before: H and O<sub>2</sub>,<sup>21</sup> OH groups,<sup>22</sup> SO<sub>2</sub>,<sup>23</sup> etc. Raj *et al.*<sup>24</sup> conducted a combined theoretical and experimental XPS and IR spectral study on sulfated and phosphated TiO<sub>2</sub>. In our work we concentrate not only on the nanoclusters' structure, but on their electronic and optical properties as well. One of the main manufacturing methods of TiO<sub>2</sub> is based on the reaction with sulfuric acid where SO<sub>4</sub> groups play a significant role. Sulfate adsorption can also enhance the photoactivity of anatase to the longer wavelengths, which is profitable in hydrogen production.<sup>25</sup> SO<sub>4</sub> groups play an important role in the catalytic properties of metal oxides<sup>26–29</sup> and in solid superacids.<sup>30</sup>

Studying the particles of nanosize experimentally could be a demanding task where computational methods come into help. DFT has proven to be a very efficient and accurate method given that the exchange–correlation functional is chosen wisely. This theoretical approach yields reproducible results, as was shown recently for single-element solids using the PBE functional.<sup>31</sup> Our study can shed light on the effect of the surrounding media on the particles' properties, and the results can be used in the computational modeling of TiO<sub>2</sub> nanoparticles even though many other adsorbates besides SO<sub>4</sub> can be present on the surface of the nanoparticles simultaneously, and in real life applications particles are at a temperature higher than 0 K.

Our model structure was chosen to be a TiO<sub>2</sub> anatase cluster consisting of 16TiO<sub>2</sub> units, carved from the experimental bulk crystal by stripping off TiO<sub>2</sub> units to maintain the stoichiometry and sufficiently high coordination of all constituent atoms. This approach was adopted from the work of Persson *et al.*<sup>32</sup> This particular size was chosen because it is large enough to have a distinguishable anatase structure, but small enough for the calculations to be feasible. In our previous work<sup>33</sup> two different particle shapes were studied: spherical and needle-like to simulate the types of particles that form during the manufacturing process. The study showed that the most symmetrical,

<sup>a</sup> University of Oulu, Theoretical Physics Research Unit, PL 3000, FI-90014 Oulu, Finland. E-mail: olga.miroshnichenko@oulu.fi

<sup>b</sup> Peter the Great St. Petersburg Polytechnic University, Department of Theoretical Mechanics, Polytechnicheskaya 29, 195251 St. Petersburg, Russian Federation

† Electronic supplementary information (ESI) available. See DOI: 10.1039/c6cp05681d



spherical particles of anatase are more stable as opposed to needle-like structures, and therefore a spherical particle shape was chosen for this work. To find the structure of  $(\text{TiO}_2)_{16}$  no global optimization method was used.

## 2 Computational details

All calculations in this study were performed using the DFT-based GPAW software package<sup>34–36</sup> in the real-space implementation of the projector-augmented wave (PAW) method.<sup>37,38</sup> All structures were treated as spin-paired and charge neutral. Calculations were performed in the finite difference mode at 0 K electronic temperature using only the  $\Gamma$ -point. The Perdew, Burke, Ernzerhof (PBE) exchange–correlation functional was used in all calculations.

For structural relaxation, the computational box was set without periodic boundary conditions, with 7 Å of vacuum surrounding the structure. The real space grid spacing of 0.17 Å was used. Relaxations were performed using a quasi-Newton minimizer until all forces were smaller than  $0.01 \text{ eV \AA}^{-1}$ .

The density of states (DOS) and local density of states (LDOS) were calculated using the same settings as the relaxation runs, except that the empty states were also required to be fully converged up to the ten highest bands. DOS and LDOS plots were obtained using 2000 data points and a normalized Gaussian broadening of 0.1 eV.

Bader charge analysis<sup>39–42</sup> was performed using the all electron density obtained with a grid refinement equal to 4.

Due to the known shortcomings of the standard DFT+PBE method yielding band gaps smaller than the experimental values, the DFT+U test calculations were done previously for the anatase  $(\text{TiO}_2)_{38}$  structure, with the values of  $U = 2, 3, 6, 6.8,$  and  $10 \text{ eV}$ .<sup>43</sup> The tests showed that  $U$  correction did not result in a significantly larger band gap than the standard PBE calculation, and both methods showed the defect states appearing at the same positions. Calculations using the hybrid functional should yield a more accurate electronic structure,<sup>44</sup> but were not tested in this work due to software limitations.

Photoabsorption spectra calculations were performed using a time-propagation time-dependent DFT (TP-TDDFT) approach<sup>45</sup> in GPAW using a 16.0 attosecond time step with 1000 iterations resulting in a total simulation time of 16 femtoseconds. The delta absorption kick for the initial disturbance of wave functions was set to  $10^{-3}$ . TDDFT calculations were performed using non-periodic boundary conditions and 10 Å of empty space around the clusters in every coordinate direction. To save computational time, a bigger grid spacing of 0.3 Å was used. This value was tested in our previous work,<sup>33</sup> giving well-converged eigenvalues for bands in the absorption region. The spectra were calculated from the dipole moment files with a 0.1 eV Gaussian broadening.

Adsorption energies per sulfate group were calculated using the formula:

$$E_{\text{ads}} = (N \times E_{\text{SO}_4} + E_{\text{cluster}} - E_{\text{cluster}+N \times \text{SO}_4})/N,$$

where  $N$  is the number of  $\text{SO}_4$  groups on the surface of the anatase cluster;  $E_{\text{SO}_4}$ ,  $E_{\text{cluster}}$  are the ground state energies of the

isolated  $\text{SO}_4$  and  $\text{Ti}_{16}\text{O}_{32}$  clusters, respectively;  $E_{\text{cluster}+N \times \text{SO}_4}$  is the total energy of the cluster with adsorbed sulfate groups after geometry optimization.

## 3 Results and discussion

### 3.1 Structural effects

The effect of  $\text{SO}_4$  groups was studied on a relaxed stoichiometric  $\text{Ti}_{16}\text{O}_{32}$  anatase cluster with the  $C_i$  point group (Fig. 1a and b). Due to the mentioned symmetry, half of the Ti atoms have the same coordination and bonding environment as the other diametrically opposite half relative to the inverse center, which in this case is a geometric center. In the literature it is suggested that  $\text{SO}_4$  groups attach to two surface titanium atoms through sulfate's single-bonded oxygens.<sup>24,25,30</sup> To find the most favorable site for the adsorption of the  $1\text{SO}_4$  group, it was attached to all reasonable and nonidentical Ti pairs on the edge and at the center of the cluster, resulting in 9 different configurations. These configurations were subsequently relaxed in GPAW and the lowest energy structure was found (Fig. 1c and d) with the energy difference from the structure with the highest energy equal to 2.33 eV.

For the adsorption of  $2\text{SO}_4$  groups, sulfates were attached to all reasonable and symmetrical Ti pairs, resulting in 9 different configurations with a maximum energy difference for relaxed structures equal to 3.59 eV. The lowest energy structure is depicted in Fig. 1e and f. Configurations for the adsorption of  $3\text{SO}_4$  and  $4\text{SO}_4$  groups were chosen on the basis of  $2\text{SO}_4$  group structures with minimal, maximal, and average energies. The additional one  $\text{SO}_4$  group for the adsorption study of  $3\text{SO}_4$  groups (two  $\text{SO}_4$  groups for  $4\text{SO}_4$ ) was added to the structures in a reasonable and symmetrical manner, resulting in 34 configurations with a maximum energy difference of 4.61 eV (18 configurations for  $\text{Ti}_{16}\text{O}_{32} + 4\text{SO}_4$  with the energy difference equal to 4.13 eV). Relaxed lowest energy structures for a cluster with 3 and 4 sulfates adsorbed are depicted in Fig. 1g–l. The studied configurations do not include all possible ones, and the obtained minimum energy structures are not necessarily the most stable configurations, but the number of the structures studied had to be limited due to the amount of computational time needed to perform the calculations. We could not find the experimental information on the adsorption site of the  $\text{SO}_4$  groups on the  $\text{TiO}_2$  clusters of size comparable to that of our model system.

In Table 1 adsorption bond lengths for  $\text{SO}_4$  groups, which are the distances between single bonded O atoms from sulfates and Ti atoms to which they are attached, and adsorption energies per  $\text{SO}_4$  group, are tabulated. It is interesting to note that in the case of an odd number of sulfate groups the adsorption energy is higher than in the even case. The case with  $1\text{SO}_4$  group adsorption shows the shortest bond lengths and has the highest adsorption energy. Adding more sulfate groups elongates the adsorption bond lengths, and in these cases the adsorption energies are lower. To understand the electronic charge transfer between the  $\text{SO}_4$  groups and the



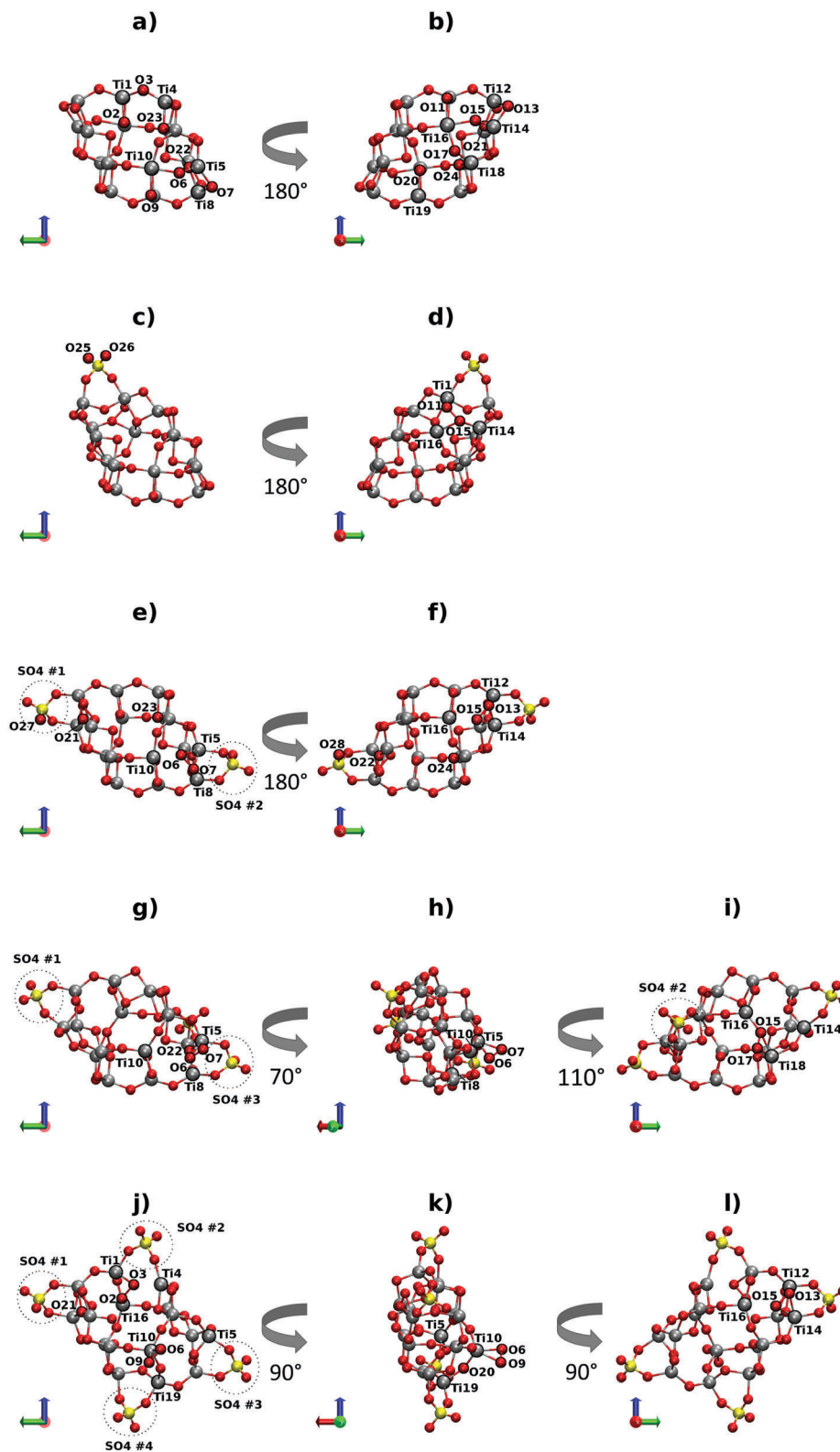


**Fig. 1** The relaxed cluster structures: (a) bare  $\text{Ti}_{16}\text{O}_{32}$ , (b) bare  $\text{Ti}_{16}\text{O}_{32}$  turned by  $180^\circ$  around the z axis relative to (a), (c)  $\text{Ti}_{16}\text{O}_{32}$  with the 1 $\text{SO}_4$  group, (d)  $\text{Ti}_{16}\text{O}_{32}$  with the 1 $\text{SO}_4$  group turned by  $180^\circ$  around the z axis relative to (c), (e)  $\text{Ti}_{16}\text{O}_{32}$  with 2 $\text{SO}_4$  groups, (f)  $\text{Ti}_{16}\text{O}_{32}$  with 2 $\text{SO}_4$  groups turned by  $180^\circ$  around the z axis relative to (e), (g)  $\text{Ti}_{16}\text{O}_{32}$  with 3 $\text{SO}_4$  groups, (h)  $\text{Ti}_{16}\text{O}_{32}$  with 3 $\text{SO}_4$  groups turned by  $70^\circ$  around the z axis relative to (g), (i)  $\text{Ti}_{16}\text{O}_{32}$  with 3 $\text{SO}_4$  groups turned by  $110^\circ$  around the z axis relative to (h), (j)  $\text{Ti}_{16}\text{O}_{32}$  with 4 $\text{SO}_4$  groups, (k)  $\text{Ti}_{16}\text{O}_{32}$  with 4 $\text{SO}_4$  groups turned by  $90^\circ$  around the z axis relative to (j), and (l)  $\text{Ti}_{16}\text{O}_{32}$  with 4 $\text{SO}_4$  groups turned by  $90^\circ$  around the z axis relative to (k). Oxygen atoms are marked with red color, titanium atoms as gray color, and sulfur atoms are yellow. The red, green, and blue coordinate axes represent x, y, and z axes, respectively.



**Table 1** SO<sub>4</sub> group adsorption bond lengths, adsorption energies per SO<sub>4</sub> group, and Bader partial charges per SO<sub>4</sub> group

Structure	Ti–O <sub>SO<sub>4</sub></sub> /Å	Avg./Å	E <sub>ads</sub> /eV	Charge/e	Avg./e
Ti <sub>16</sub> O <sub>32</sub> + 1SO <sub>4</sub>	1.884	1.877	3.824	–1.247	–1.247
	1.870				
Ti <sub>16</sub> O <sub>32</sub> + 2SO <sub>4</sub>	1.903	1.895	3.374	–1.272	–1.274
	1.892				
	1.899				
	1.887				
Ti <sub>16</sub> O <sub>32</sub> + 3SO <sub>4</sub>	1.938	1.930	3.488	–1.182	–1.102
	1.882				
	1.971				
	1.990				
	1.900				
	1.896				
Ti <sub>16</sub> O <sub>32</sub> + 4SO <sub>4</sub>	1.903	1.902	3.230	–1.095	–1.145
	1.911				
	1.938				
	1.875				
	1.878				
	1.907				
	1.933				
1.868					

clusters, the Bader charges were calculated. The partial charges for SO<sub>4</sub> groups are negative, meaning that the sulfates steal electrons from the cluster, which is consistent with the literature.<sup>25</sup>

To understand the effect of SO<sub>4</sub> groups on the structure of the Ti<sub>16</sub>O<sub>32</sub> clusters the bonding environment and the clusters'

**Table 2** Number of bonds in the relaxed structures. The SO<sub>4</sub> groups are not taken into account

Structure	n <sub>Ti–O</sub>	n <sub>Ti–Ti</sub>	n <sub>O–O</sub>	n <sub>All</sub>
Ti <sub>16</sub> O <sub>32</sub> bare	68	12	—	80
Ti <sub>16</sub> O <sub>32</sub> + 1SO <sub>4</sub>	70	11	1	82
Ti <sub>16</sub> O <sub>32</sub> + 2SO <sub>4</sub>	66	10	2	78
Ti <sub>16</sub> O <sub>32</sub> + 3SO <sub>4</sub>	64	9	2	75
Ti <sub>16</sub> O <sub>32</sub> + 4SO <sub>4</sub>	62	7	3	72

**Table 3** Average bond lengths in the relaxed structures. The SO<sub>4</sub> groups are not taken into account

Structure	d <sub>Ti–O</sub> /Å	d <sub>Ti–Ti</sub> /Å	d <sub>O–O</sub> /Å	d <sub>All</sub> /Å
Ti <sub>16</sub> O <sub>32</sub> bare	1.872	2.789	—	2.009
Ti <sub>16</sub> O <sub>32</sub> + 1SO <sub>4</sub>	1.900	2.814	1.492	2.018
Ti <sub>16</sub> O <sub>32</sub> + 2SO <sub>4</sub>	1.883	2.803	1.473	1.990
Ti <sub>16</sub> O <sub>32</sub> + 3SO <sub>4</sub>	1.880	2.815	1.393	1.979
Ti <sub>16</sub> O <sub>32</sub> + 4SO <sub>4</sub>	1.878	2.850	1.418	1.953

**Table 4** Dimensions of the clusters without taking into account SO<sub>4</sub> groups in three coordinate directions (x, y, and z) and the average dimension (values in the parenthesis are dimensions calculated by taking into account SO<sub>4</sub> groups)

Structure	x/Å	y/Å	z/Å	Avg./Å
Ti <sub>16</sub> O <sub>32</sub> bare	6.093	10.715	8.352	8.387
Ti <sub>16</sub> O <sub>32</sub> + 1SO <sub>4</sub>	6.345	10.660	8.779 (11.612)	8.595 (9.539)
Ti <sub>16</sub> O <sub>32</sub> + 2SO <sub>4</sub>	6.148	9.371 (16.998)	8.493	8.004 (10.546)
Ti <sub>16</sub> O <sub>32</sub> + 3SO <sub>4</sub>	6.476 (9.359)	10.997 (16.946)	9.077	8.850 (11.794)
Ti <sub>16</sub> O <sub>32</sub> + 4SO <sub>4</sub>	8.295	10.493 (16.860)	8.771 (14.947)	9.186 (13.367)

dimensions were studied. All information was gathered in Tables 2–6. In the bonding analysis we used the same cut-off radii as in our previous work:<sup>22</sup> 2.2 Å for Ti–O bonds, 2.94 Å for Ti–Ti, except for the O–O bonds the cut-off radius was set to 1.5 Å, to take into account clear bonding between some of the oxygens (see Section 3.2). The number of all bonds in the structures is gathered in Table 2. Note that in Tables 2–4 the SO<sub>4</sub> groups were not taken into account (bonds in SO<sub>4</sub> groups and bonds between the cluster and the SO<sub>4</sub> groups) to concentrate on the structural changes in the cluster structures. It can be seen that sulfates deform the structure of the underlying cluster, resulting in a decreased number of Ti–Ti bonds, but also in the appearance of O–O bonds. The number of Ti–O bonds is decreasing upon sulfate adsorption, with the 1SO<sub>4</sub> case as an exception. The average bond lengths are reported in Table 3. The averages of all bond lengths tend to decrease upon sulfate adsorption even though average Ti–O and Ti–Ti bonds are elongated. It can be explained by the appearance of an increasing number of relatively short O–O bonds in the clusters, resulting from an increasing number of sulfate groups on the surface. The average of all bond lengths in the case with the 1SO<sub>4</sub> group does not follow the tendency of getting smaller, in this case the Ti–O average bond length is significantly longer than in the bare cluster, and the new O–O bond is relatively long.

The dimensions of the structures were calculated as the longest distances between the atoms in three coordinate directions. They are tabulated in Table 4, where the values in parentheses represent the dimensions of the cluster calculated with SO<sub>4</sub> taken into account to show in which coordinate directions the SO<sub>4</sub> groups were oriented. The average dimensions are increasing, except for the structure with 2SO<sub>4</sub> groups. In this case the y dimension is contracted significantly due to the repelling effect of the SO<sub>4</sub> groups oriented in this direction, causing the outermost oxygen atoms in the cluster corners to move inside the cluster. In the case of the adsorption of 3 and 4SO<sub>4</sub> groups, 2 of the sulfates are also oriented in the y direction, but this dimension does not decrease dramatically (or even increases in the 3SO<sub>4</sub> case) probably due to other structural distortions occurring in the cluster. Configurations with 3 and 4 sulfate groups have enlarged x dimensions due to the formation of side-on coordinated O–O species ( $\eta^2$ -O<sub>2</sub>, where  $\eta$  stands for the hapticity of O–O),<sup>46,47</sup> pointing in this direction (Fig. 1 O6 and O7 in g and h, O6 and O9 in j and k). We believe that the appearance of O–O bonds in the structures with adsorbed SO<sub>4</sub> groups deserves to be studied in more detail. Furthermore, Albaret *et al.* reported the appearance of O–O bonds in the small O-rich TiO<sub>2</sub> clusters.<sup>48</sup> Structures with adsorbed SO<sub>4</sub>



**Table 5** Calculated bond lengths and Bader charges of the O–O species

Structure	Atoms	Bond length/Å	Charge/e
Ti <sub>16</sub> O <sub>32</sub> + 1SO <sub>4</sub>	O11–O15	1.492	−1.215
Ti <sub>16</sub> O <sub>32</sub> + 2SO <sub>4</sub>	O13–O15	1.473	−1.099
	O6–O7	1.474	−1.100
Ti <sub>16</sub> O <sub>32</sub> + 3SO <sub>4</sub>	O15–O17	1.442	−1.050
Ti <sub>16</sub> O <sub>32</sub> + 3SO <sub>4</sub>	O6–O7 (η <sup>2</sup> -O <sub>2</sub> )	1.345	−0.556
Ti <sub>16</sub> O <sub>32</sub> + 4SO <sub>4</sub>	O13–O15	1.455	−1.051
Ti <sub>16</sub> O <sub>32</sub> + 4SO <sub>4</sub>	O2–O3	1.471	−1.148
Ti <sub>16</sub> O <sub>32</sub> + 4SO <sub>4</sub>	O6–O9 (η <sup>2</sup> -O <sub>2</sub> )	1.327	−0.452

groups could be treated as O-rich clusters; therefore, O–O bond lengths and Bader charges per O–O species are documented in Table 5. Bond lengths of η<sup>2</sup>-O<sub>2</sub> species are significantly shorter than other O–O bond lengths. Apparently, charge transfer from the cluster to the η<sup>2</sup>-O<sub>2</sub> is smaller than in other O–O bonds. This fact is supported by the elongated Ti–O bonds in these cases: Ti5–O6 and Ti5–O7 bonds are 1.995 Å and 1.98 Å, respectively, which is 0.115 and 0.1 Å longer than the average Ti–O bond lengths in the structure with 3SO<sub>4</sub> groups; Ti10–O9 and Ti10–O6 bonds are 2.038 Å and 2.037 Å, respectively, which is 0.16 and 0.159 Å longer than the average Ti–O bond lengths in the structure with 4SO<sub>4</sub> groups. According to the abovementioned facts, η<sup>2</sup>-O<sub>2</sub> species exhibit superoxo characteristics.<sup>46,47</sup>

To verify that the appearance of O–O bonds is not a shortcoming of our model, other models were considered. In real life conditions clusters should reside in water. However, surrounding the whole cluster with water molecules would significantly increase the computational burden. For this reason, calculations for the cluster with 1 adsorbed SO<sub>4</sub> group and with 3–7 water molecules placed around the SO<sub>4</sub> were performed. In all cases the O–O bonds between the O11 and O15 atoms eventually appeared, which served as a reason for us to stop the calculations before convergence was reached, since relaxations caused the formation of the same O–O bonds as in the structures without water molecules. To improve the model further, one could use the continuum solvent method,<sup>49</sup> which was recently implemented in GPAW, but it is out of scope of this work.

Coordinations of atoms were calculated and the results are summarized in Table 6. The bonds between sulfates and titanium atoms to which they had been attached were taken into account, only bonds in SO<sub>4</sub> groups were neglected. The normal coordination for Ti is 6 and for O is 3.<sup>50</sup> In the structures with 3 and 4 sulfates strongly undercoordinated Ti atoms appear. As will be seen further in Section 3.2, these are the structures that exhibit defect states in the band gap.

**Table 6** Coordination of Ti and O atoms in the relaxed clusters. Atoms in the SO<sub>4</sub> groups are not taken into account

Structure	4f-Ti	5f-Ti	6f-Ti	7f-Ti	2f-O	3f-O
Ti <sub>16</sub> O <sub>32</sub> bare	—	6	8	2	28	4
Ti <sub>16</sub> O <sub>32</sub> + 1SO <sub>4</sub>	—	7	4	5	24	8
Ti <sub>16</sub> O <sub>32</sub> + 2SO <sub>4</sub>	—	8	6	2	26	6
Ti <sub>16</sub> O <sub>32</sub> + 3SO <sub>4</sub>	2	7	4	3	28	4
Ti <sub>16</sub> O <sub>32</sub> + 4SO <sub>4</sub>	3	8	3	2	28	4

The number of undercoordinated Ti atoms increases upon adding more sulfates from 6 for bare cluster to 11 in the structure with 4SO<sub>4</sub> groups.

### 3.2 Electronic properties

Densities of states were calculated for all structures and depicted in Fig. 2. The DOS were plotted relative to the Fermi level of the bare cluster. Electronic structure information is collected in Table 7. The band gap of the bare cluster is 0.7 eV larger than the computed band gap of the bulk anatase (2.12 eV),<sup>33</sup>

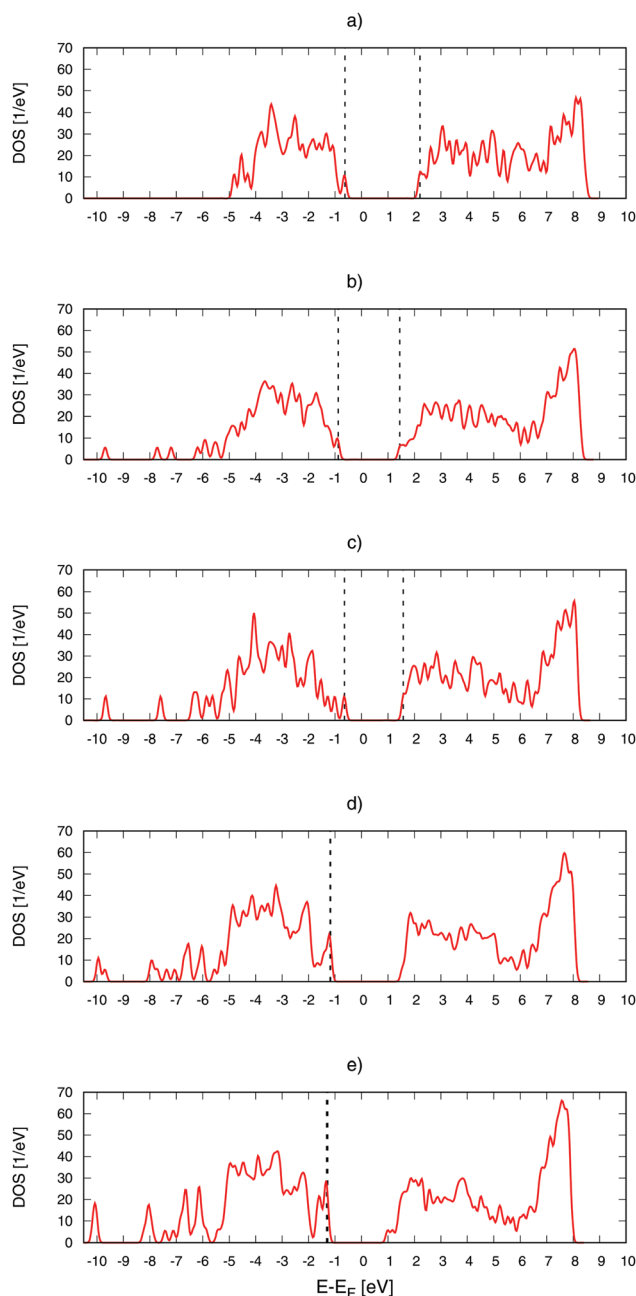


**Fig. 2** DOS for (a) bare Ti<sub>16</sub>O<sub>32</sub>, (b) Ti<sub>16</sub>O<sub>32</sub> with the 1SO<sub>4</sub> group, (c) with 2SO<sub>4</sub> groups, (d) 3SO<sub>4</sub> groups, and (e) Ti<sub>16</sub>O<sub>32</sub> with 4SO<sub>4</sub> groups relative to the Fermi level of bare Ti<sub>16</sub>O<sub>32</sub>. HOMO and LUMO levels are plotted with vertical dashed lines. In (d) and (e) HOMO and LUMO levels almost coincide.



**Table 7** Band gap and HOMO–LUMO energies in eV for relaxed clusters. The zero energy level is shifted to the Fermi level of the bare  $\text{Ti}_{16}\text{O}_{32}$  cluster

Structure	HOMO	LUMO	$\Delta_{\text{HOMO-LUMO}}$
$\text{Ti}_{16}\text{O}_{32}$ bare	−0.626	2.207	2.833
$\text{Ti}_{16}\text{O}_{32} + 1\text{SO}_4$	−0.880	1.448	2.328
$\text{Ti}_{16}\text{O}_{32} + 2\text{SO}_4$	−0.643	1.577	2.220
$\text{Ti}_{16}\text{O}_{32} + 3\text{SO}_4$	−1.190	−1.167	0.023 (2.753 <sup>a</sup> )
$\text{Ti}_{16}\text{O}_{32} + 4\text{SO}_4$	−1.320	−1.274	0.046 (2.327 <sup>a</sup> )

<sup>a</sup> The HOMO–LUMO difference was calculated as the difference between the edges of valence and conduction bands.

which is consistent with the reported blue-shifts of 0.1–0.6 eV for quantum sized  $\text{TiO}_2$  particles.<sup>51</sup> The band gap of bulk anatase computed using the PBE functional is underestimated by about 1 eV, but it gives correct band gap energy differences for three  $\text{TiO}_2$  polymorphs.<sup>33</sup> Dashed lines represent the Highest Occupied Molecular Orbital (HOMO) and Lowest Unoccupied Molecular Orbital (LUMO) levels. In the case of the adsorption of 3 and 4 sulfates these levels are almost identical, resulting in a very small HOMO–LUMO difference. The fundamental band gap was estimated as the difference between the bottom peak of the conduction band and the top peak of the valence band in these cases (values in parentheses in Table 7). The relaxation process caused the appearance of O–O bonds in the structures according to our structural analysis. Local densities of states were calculated for these oxygens' p-orbitals to prove the existence of these bonds (Fig. 3 and 4 and Fig. S1–S6 in the ESI†). Additionally, the LDOS for their Ti neighbors' d-orbitals were plotted to get an understanding of how O atoms are bonded to Ti atoms before and after sulfate adsorption.

Adding one  $\text{SO}_4$  group lowers the separation between the HOMO and LUMO levels by 0.5 eV and introduces new states at the bottom of the valence band (Fig. 2b). The new peaks are formed by orbitals of the sulfur atom and O11–O15 atoms (Fig. 1d). The detailed list of the new peaks and atoms contributing to them is documented in Table S1 (ESI†). O11 and O15

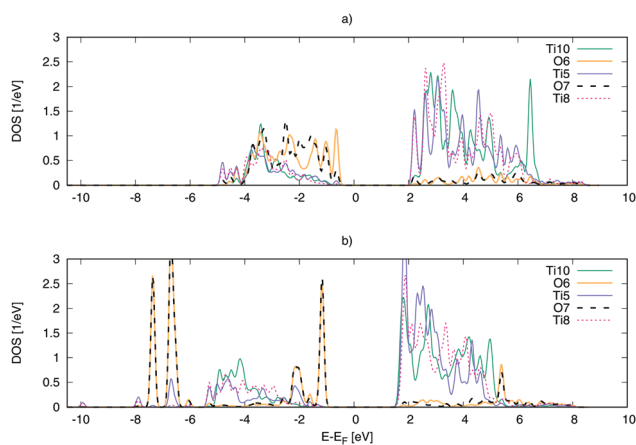


**Fig. 3** LDOS before (a) and after (b) the adsorption of 3 $\text{SO}_4$  groups for the p-orbitals of O atoms, forming the O–O bond and the d-orbitals of neighboring Ti atoms. The atoms are shown in Fig. 1g and h.

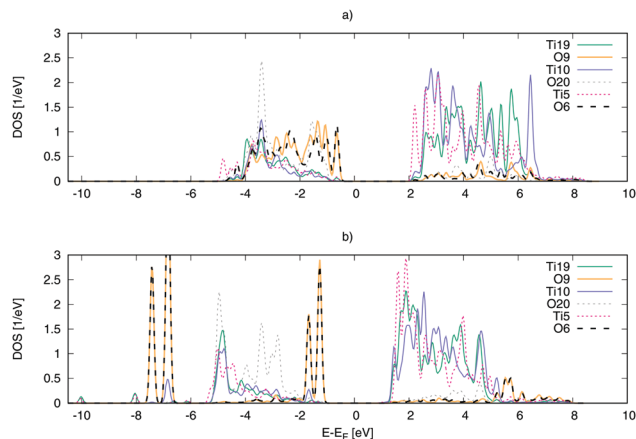


**Fig. 4** LDOS before (a) and after (b) the adsorption of 4 $\text{SO}_4$  groups for the p-orbitals of O atoms, forming the O–O bond, and the d-orbitals of neighboring Ti atoms. The atoms are shown in Fig. 1j and k.

form a bond after 1 $\text{SO}_4$  adsorption, which is supported by a strong hybridization of their p-orbitals (Fig. S1, ESI†). The HOMO level consists of p-orbitals of double-bonded O atoms in the  $\text{SO}_4$  group (O25 and O26), the LUMO is on the d-orbital of Ti1, one of the atoms to which the sulfate group is attached (Fig. 1c and d). The right edge of the conduction band has an increased DOS intensity, caused mostly by the p-orbital of the S atom.

The adsorption of 2 $\text{SO}_4$  groups causes the contraction of the HOMO–LUMO difference by 0.6 eV. New states appear at the bottom of the valence band due to atoms in  $\text{SO}_4$  groups, atoms to which  $\text{SO}_4$  groups are attached, and oxygens forming O–O bonds. The details about new states can be found in Table S2 (ESI†). The p-orbitals of O6–O7 and O15–O13, which are forming the O–O bonds (Fig. 1e and f), show strong hybridization (Fig. S2 and S3, ESI†). The HOMO level is located on O13, O7, O15 and O6-atoms, forming the O–O bonds after relaxation. The LUMO level is on the Ti atoms, to which different  $\text{SO}_4$  groups are attached (Ti8 and Ti12, Fig. 1e and f). The DOS intensity at the top of the conduction band increases with major contribution from the p-orbitals of the sulfur atoms.

Three  $\text{SO}_4$  groups adsorbed on the surface of the  $\text{Ti}_{16}\text{O}_{32}$  cluster cause the defect state at the top of the valence band, resulting in an almost negligible HOMO–LUMO difference. Nevertheless, the actual valence-conduction band separation estimated from the DOS plot is as big as 2.753 eV (Table 7), which is only 0.1 eV lower than in the bare cluster. The defect unoccupied state is situated on the p-orbitals of O6 and O7-atoms, forming the  $\eta^2\text{-O}_2$  structure (Fig. 1g and h). The p-orbitals of these oxygens have a strongly localized character, as in a molecule, having very weak hybridization with the Ti5 atom to which they are attached (Fig. 3). As in the previous cases, new states appear at the lower part of the valence band mostly due to the atoms from  $\text{SO}_4$  groups, atoms to which  $\text{SO}_4$  groups are attached, and oxygens forming O–O bonds and  $\eta^2\text{-O}_2$ . The detailed information about new states is documented in Table S3 (ESI†). The HOMO level is on the p-orbitals of O7 and O6 ( $\eta^2\text{-O}_2$ ), and on the p-orbital of O17



from the O–O bond. The state at the bottom of the conduction band is situated on the d-orbital of Ti18, *i.e.* the Ti atom, to which O15–O17 is connected (Fig. 1i). The top part of the conduction band, where the increase of the DOS intensity is observed, is mostly formed by the p-orbitals of the sulfur atoms.

Four SO<sub>4</sub> groups cause a 0.5 eV contraction of the fundamental band gap, but the HOMO–LUMO gap is very small because of the defect unoccupied state at –1.274 eV due to the p-orbitals of O9 and O6 (Fig. 1j and k), which form the  $\eta^2$ -O<sub>2</sub> structure with localized states as can be seen in the LDOS pictures (Fig. 4). The states at the bottom of the valence band appear mostly due to the atoms from SO<sub>4</sub> groups, atoms to which SO<sub>4</sub> groups are attached, and oxygens forming O–O bonds and  $\eta^2$ -O<sub>2</sub> (Table S4, ESI†). The HOMO level is formed by the p-orbitals of O9 and O6 in the  $\eta^2$ -O<sub>2</sub> species. The bottom of the conduction band is formed by the d-orbital of Ti16. The top edge of the conduction band is formed mostly by the p-orbitals of the sulfur atoms.

The same analysis was performed for the bare cluster for comparison. In the bare cluster the HOMO level is situated on the p-orbitals of O15 and O6 (Fig. 1a and b), the LUMO is on the d-orbitals of Ti14, Ti5, Ti12, and Ti8, which are at the corners of the cluster. The top part of the conduction band does not have any predominant atom contributions to the DOS.

A comparison of all the electronic structures studied can be summarized so that the SO<sub>4</sub> groups cause the appearance of new states at the bottom of the valence band, formed mostly by atoms in SO<sub>4</sub> groups, atoms to which these groups are attached, and oxygen atoms, forming O–O bonds and  $\eta^2$ -O<sub>2</sub>. The DOS at the top of the conduction band has an increased intensity upon sulfate adsorption due to the contribution of S atoms. In the structures, where the defect empty state appears at the top of the valence band, the HOMO and LUMO levels consist of the orbitals of O atoms, which form the bonds and  $\eta^2$ -O<sub>2</sub> structures after relaxation. This is consistent with the findings of Martinez *et al.* for the SrTiO<sub>3</sub> surface, where states near the Fermi level are mostly derived from adsorbate  $\eta^2$ -O<sub>2</sub> orbitals.<sup>46</sup>

### 3.3 Optical properties

The photoabsorption spectra in three coordinate directions and the total averaged spectra were calculated for all structures and are presented in Fig. 5a–d. The absorption shoulder for the clusters starts at approximately 3 eV. For bigger nanoparticles the experimental absorption edge was reported to be 3–3.55 eV.<sup>52–55</sup> The results for the electronic structure are reflected also in the spectra: for the clusters with defect states in the band gap and negligible HOMO–LUMO differences absorption starts already at very low energies, which can be seen in the magnified pictures in the insets. The largest adsorption intensity in the low energy region for Ti<sub>16</sub>O<sub>32</sub> + 3SO<sub>4</sub> and 4SO<sub>4</sub> is observed in the *x*-coordinate direction. It is the direction in which the  $\eta^2$ -O<sub>2</sub> bonds are pointing (Fig. 1g, h and j, k). We could not find experimental data for the adsorption in the low energy region for small TiO<sub>2</sub> clusters with SO<sub>4</sub> groups. The most photoactive direction is *z*, where the intensity of absorption is about 12 eV<sup>-1</sup>, and the least active is *x*, where the intensity is about 8–9 eV<sup>-1</sup>.

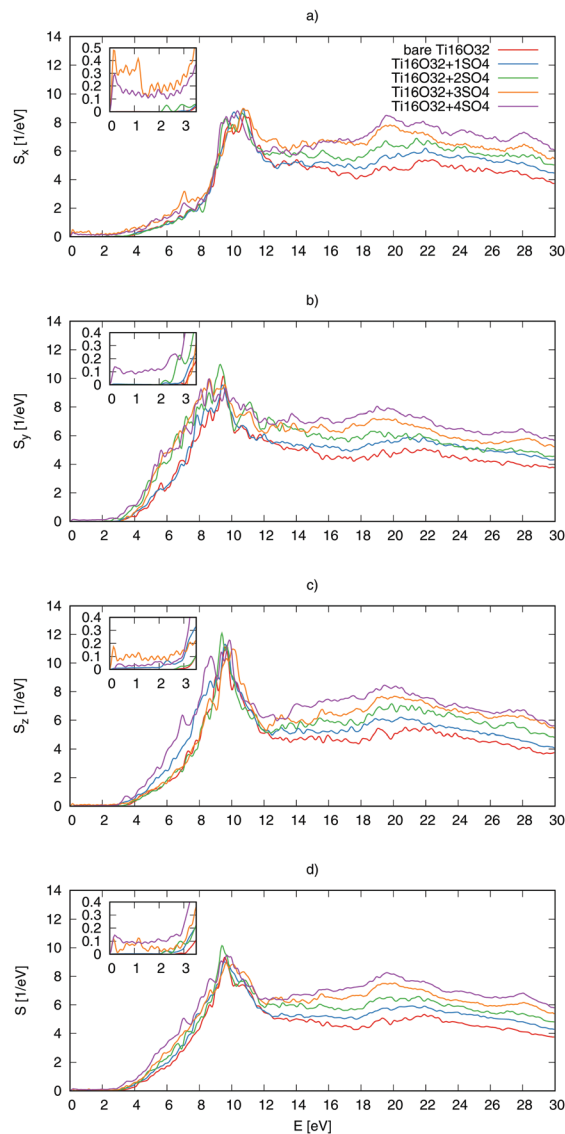


Fig. 5 (a) Photoabsorption spectrum for the *x* coordinate direction, (b) for the *y* coordinate direction, (c) for the *z*, and (d) total averaged photoabsorption spectra for the bare Ti<sub>16</sub>O<sub>32</sub> structure, Ti<sub>16</sub>O<sub>32</sub> with the 1SO<sub>4</sub> group, with 2SO<sub>4</sub> groups, 3SO<sub>4</sub> groups, and with 4SO<sub>4</sub> groups. The low energy region is magnified in the insets.

From the total photoabsorption spectra (Fig. 5d) it can be seen that the adsorption of SO<sub>4</sub> groups enhances adsorption in the energy ranges: 3–9 eV and 12–30 eV. The amplitude increases monotonically upon SO<sub>4</sub> group adsorption, especially in the high energy region.

## 4 Conclusions

The effect of SO<sub>4</sub> group adsorption on the geometry, electronic structure, and photoabsorption spectrum of Ti<sub>16</sub>O<sub>32</sub> nanoparticles has been studied. The results show that sulfates tend to break or elongate Ti–Ti bonds and introduce O–O bonds into the structures. In the cases of 3 and 4SO<sub>4</sub> groups side-on coordinated  $\eta^2$ -O<sub>2</sub> structures appear, which is interesting



because they are intermediate species in the production of molecular oxygen from water on transition metal based oxides.<sup>46</sup> The number of Ti–O bonds and the overall number of bonds tend to decrease upon SO<sub>4</sub> group adsorption, with an exception in the case of 1SO<sub>4</sub> group adsorption. The sulfate groups introduce new states at the bottom of the valence band (from –10 eV to –5 eV). In the case of 3 and 4SO<sub>4</sub> groups, the oxygen atoms from the η<sup>2</sup>-O<sub>2</sub> species cause the appearance of an empty state at the top of the valence band, resulting in an almost negligible HOMO–LUMO difference. The orbitals of these atoms also contribute to the formation of new states at the bottom of the valence band. The DOS intensity is enhanced at the top of the conduction band due to the contribution of sulfur atoms. The trend in the electronic structure is also observed in the optical properties. The absorption intensity is larger at higher energies (12–30 eV) for structures with SO<sub>4</sub> groups on the surface, and for structures with 3 and 4 adsorbed sulfates photoabsorption starts already at very small energies. The results indicate the importance of taking into account the effect of the surrounding media and the SO<sub>4</sub> groups in particular when comparing the results of computational modeling with experiments performed for TiO<sub>2</sub> nanoparticles, and the results could be used for the photocatalytic application of TiO<sub>2</sub> clusters.

## Acknowledgements

We want to acknowledge PhD Juho-Pertti Jalava from ProfMath Oy, PhD Ralf-Johan Lamminmäki, and MSc Minna Lindholm from Huntsman Pigments, Pori, Finland, Dr Erik Vartiainen and Prof. Heikki Haario from Lappeenranta University of Technology, and PhD Veli-Matti Taavitsainen from Helsinki Metropolia University for their comments. The computational resources were provided by CSC-Scientific Computing Ltd, Espoo, Finland.

## References

- 1 A. Fujishima and K. Honda, *Nature*, 1972, **238**, 37–38.
- 2 A. Fujishima, T. N. Rao and D. A. Tryk, *J. Photochem. Photobiol., C*, 2000, **1**, 1–21.
- 3 D. Tryk, A. Fujishima and K. Honda, *Electrochim. Acta*, 2000, **45**, 2363–2376.
- 4 A. L. Linsebigler, G. Lu and J. T. Yates, *Chem. Rev.*, 1995, **95**, 735–758.
- 5 M. R. Hoffmann, S. T. Martin, W. Choi and D. W. Bahnemann, *Chem. Rev.*, 1995, **95**, 69–96.
- 6 J. Braun, A. Baidins and R. Marganski, *Prog. Org. Coat.*, 1992, **20**, 105–138.
- 7 M. Ni, M. K. Leung, D. Y. Leung and K. Sumathy, *Renewable Sustainable Energy Rev.*, 2007, **11**, 401–425.
- 8 X. Chen and S. S. Mao, *Chem. Rev.*, 2007, **107**, 2891–2959.
- 9 R. S. Lima and B. R. Marple, *J. Therm. Spray Technol.*, 2007, **16**, 40–63.
- 10 P. Kern, P. Schwaller and J. Michler, *Thin Solid Films*, 2006, **494**, 279–286.
- 11 M. Grätzel, *Prog. Photovoltaics*, 2000, **8**, 171–185.
- 12 M. Grätzel, *Nature*, 2001, **414**, 338–344.
- 13 M. Grätzel, *J. Photochem. Photobiol., C*, 2003, **4**, 145–153.
- 14 C. Granqvist, *Adv. Mater.*, 2003, **15**, 1789–1803.
- 15 A. N. Banerjee, *Nanotechnol., Sci. Appl.*, 2011, **4**, 35–65.
- 16 A. P. Alivisatos, *Science*, 1996, **271**, 933–937.
- 17 C. Burda, X. Chen, R. Narayanan and M. A. El-Sayed, *Chem. Rev.*, 2005, **105**, 1025–1102.
- 18 A. S. Barnard and H. Xu, *ACS Nano*, 2008, **2**, 2237–2242.
- 19 H. Zhang and J. F. Banfield, *Chem. Rev.*, 2014, **114**, 9613–9644.
- 20 J. Muscat, V. Swamy and N. M. Harrison, *Phys. Rev. B: Condens. Matter Mater. Phys.*, 2002, **65**, 224112.
- 21 A. S. Andreev, V. N. Kuznetsov and Y. V. Chizhov, *J. Mol. Model.*, 2013, **19**, 5063–5073.
- 22 O. Miroshnichenko, S. Auvinen and M. Alatalo, *Phys. Chem. Chem. Phys.*, 2015, **17**, 5321–5327.
- 23 J. Baltrusaitis, P. M. Jayaweera and V. H. Grassian, *J. Phys. Chem. C*, 2011, **115**, 492–500.
- 24 K. J. A. Raj, R. Shanmugam, R. Mahalakshmi and B. Viswanathan, *Indian J. Chem., Sect. A: Inorg., Bio-inorg., Phys., Theor. Anal. Chem.*, 2010, **49**, 9–17.
- 25 X. Liu, Y. Li, S. Peng, G. Lu and S. Li, *Photochem. Photobiol. Sci.*, 2013, **12**, 1903–1910.
- 26 K. Tanabe, M. Itoh, K. Morishige and H. Hattori, *Stud. Surf. Sci. Catal.*, 1976, **1**, 65–78.
- 27 K. Tanabe, A. Kayo and T. Yamaguchi, *J. Chem. Soc., Chem. Commun.*, 1981, **12**, 602–603.
- 28 T. Yamaguchi, T. Jin and K. Tanabe, *J. Phys. Chem.*, 1986, **90**, 3148–3152.
- 29 O. Saur, M. Bensitel, A. Saad, J. Lavalley, C. P. Tripp and B. Morrow, *J. Catal.*, 1986, **99**, 104–110.
- 30 H. Yang, R. Lu and L. Wang, *Mater. Lett.*, 2003, **57**, 1190–1196.
- 31 K. Lejaeghere, G. Bihlmayer, T. Björkman, P. Blaha, S. Blügel, V. Blum, D. Caliste, I. E. Castelli, S. J. Clark, A. Dal Corso, S. de Gironcoli, T. Deutsch, J. K. Dewhurst, I. Di Marco, C. Draxl, M. Dułak, O. Eriksson, J. A. Flores-Livas, K. F. Garrity, L. Genovese, P. Giannozzi, M. Giantomassi, S. Goedecker, X. Gonze, O. Grånäs, E. K. U. Gross, A. Gulans, F. Gygi, D. R. Hamann, P. J. Hasnip, N. A. W. Holzwarth, D. Iusan, D. B. Jochym, F. Jollet, D. Jones, G. Kresse, K. Koepnik, E. Küçükbenli, Y. O. Kvashnin, I. L. M. Locht, S. Lubeck, M. Marsman, N. Marzari, U. Nitzsche, L. Nordström, T. Ozaki, L. Paulatto, C. J. Pickard, W. Poelmans, M. I. J. Probert, K. Refson, M. Richter, G.-M. Rignanese, S. Saha, M. Scheffler, M. Schlupf, K. Schwarz, S. Sharma, F. Tavazza, P. Thunström, A. Tkatchenko, M. Torrent, D. Vanderbilt, M. J. van Setten, V. Van Speybroeck, J. M. Wills, J. R. Yates, G.-X. Zhang and S. Cottenier, *Science*, 2016, **351**, 1415.
- 32 P. Persson, J. C. M. Gebhardt and S. Lunell, *J. Phys. Chem. B*, 2003, **107**, 3336–3339.
- 33 S. Auvinen, M. Alatalo, H. Haario, J.-P. Jalava and R.-J. Lamminmäki, *J. Phys. Chem. C*, 2011, **115**, 8484–8493.
- 34 J. J. Mortensen, L. B. Hansen and K. W. Jacobsen, *Phys. Rev. B: Condens. Matter Mater. Phys.*, 2005, **71**, 035109.
- 35 J. Enkovaara, C. Rostgaard, J. J. Mortensen, J. Chen, M. Dułak, L. Ferrighi, J. Gavnholt, C. Glinsvad, V. Haikola,



- H. A. Hansen, H. H. Kristoffersen, M. Kuisma, A. H. Larsen, L. Lehtovaara, M. Ljungberg, O. Lopez-Acevedo, P. G. Moses, J. Ojanen, T. Olsen, V. Petzold, N. A. Romero, J. Stausholm-Møller, M. Strange, G. A. Tritsarlis, M. Vanin, M. Walter, B. Hammer, H. Häkkinen, G. K. H. Madsen, R. M. Nieminen, J. K. Nørskov, M. Puska, T. T. Rantala, J. Schiøtz, K. S. Thygesen and K. W. Jacobsen, *J. Phys.: Condens. Matter*, 2010, **22**, 253202.
- 36 S. R. Bahn and K. W. Jacobsen, *Comput. Sci. Eng.*, 2002, **4**, 56–66.
- 37 P. E. Blöchl, *Phys. Rev. B: Condens. Matter Mater. Phys.*, 1994, **50**, 17953–17979.
- 38 P. E. Blöchl, C. J. Först and J. Schimpl, *Bull. Mater. Sci.*, 2003, **26**, 33–41.
- 39 W. Tang, E. Sanville and G. Henkelman, *J. Phys.: Condens. Matter*, 2009, **21**, 084204.
- 40 E. Sanville, S. D. Kenny, R. Smith and G. Henkelman, *J. Comput. Chem.*, 2007, **28**, 899–908.
- 41 G. Henkelman, A. Arnaldsson and H. Jónsson, *Comput. Mater. Sci.*, 2006, **36**, 354–360.
- 42 M. Yu and D. R. Trinkle, *J. Chem. Phys.*, 2011, **134**, 064111.
- 43 S. Auvinen, M. Lahti and M. Alatalo, *Int. J. Quantum Chem.*, 2015, **115**, 1175–1180.
- 44 C. Di Valentin, G. Pacchioni and A. Selloni, *Phys. Rev. Lett.*, 2006, **97**, 166803.
- 45 M. Walter, H. Häkkinen, L. Lehtovaara, M. Puska, J. Enkovaara, C. Rostgaard and J. J. Mortensen, *J. Chem. Phys.*, 2008, **128**, 244101.
- 46 J. M. P. Martirez, S. Kim, E. H. Morales, B. T. Diroll, M. Cargnello, T. R. Gordon, C. B. Murray, D. A. Bonnell and A. M. Rappe, *J. Am. Chem. Soc.*, 2015, **137**, 2939–2947.
- 47 C. J. Cramer, W. B. Tolman, K. H. Theopold and A. L. Rheingold, *Proc. Natl. Acad. Sci. U. S. A.*, 2003, **100**, 3635–3640.
- 48 T. Albaret, F. Finocchi and C. Noguera, *J. Chem. Phys.*, 2000, **113**, 2238–2249.
- 49 A. Held and M. Walter, *J. Chem. Phys.*, 2014, **141**, 174108.
- 50 S. D. Mo and W. Y. Ching, *Phys. Rev. B: Condens. Matter Mater. Phys.*, 1995, **51**, 13023–13032.
- 51 N. Satoh, T. Nakashima, K. Kamikura and K. Yamamoto, *Nat. Nanotechnol.*, 2008, **3**, 106–111.
- 52 K. M. Reddy, C. G. Reddy and S. Manorama, *J. Solid State Chem.*, 2001, **158**, 180–186.
- 53 Y. Li, T. White and S. Lim, *J. Solid State Chem.*, 2004, **177**, 1372–1381.
- 54 S. Karthick, K. Prabakar, A. Subramania, J.-T. Hong, J.-J. Jang and H.-J. Kim, *Powder Technol.*, 2011, **205**, 36–41.
- 55 M. Pugachevskii, *Tech. Phys. Lett.*, 2013, **39**, 36–38.

